Journal of Alloys and Compounds 495 (2010) 386–390

Contents lists available at ScienceDirect

Journal of Alloys and Compounds

journal homepage: www.elsevier.com/locate/jallcom

Microstructure and mechanical properties of Al–Si–Mg ribbons

C. Triveño Rios*, M.M. Peres, C. Bolfarini, W.J. Botta, C.S. Kiminami

Materials Engineering Department, Federal University of São Carlos, S.P, Brazil

ARTICLE INFO

Article history:
Received 8 July 2008
Received in revised form 9 December 2009
Accepted 20 December 2009
Available online 28 December 2009

Keywords:
Microstructure
Mechanical properties
Quenching
Metals and alloys

ABSTRACT

In this study, the effect of the microstructural characteristics on the mechanical properties of rapidly solidified A359-type alloy was analyzed. As a result of the rapid solidification processing by melt-spinning, fine equiaxed cells grains with sizes in the range of 0.4–0.7 μm were observed in the ribbon. Heat treatment of the as melt-spun ribbon showed a growth of the nanosized Si particles from 19 nm to 80 nm (200 °C/12 h) and to 1.72 μm (450 °C/12 h). The improvement in hardness and tensile properties are related to supersaturated α-Al solid solution and to the structural refinement. The decrease in hardness and in the tensile properties after thermal ageing is attributed to Si precipitation and subsequent growth of Si particles. The as melt-spun and after heat treated at 200 °C ribbons exhibited a brittle fracture different of the after heat treated at 450 °C ribbon which showed a ductile fracture surface.

1. Introduction

Rapid solidification processing provides a typical case of non-equilibrium solidification, therefore most refined microstructures, increase in the solid solubility extension, and metastable phases formation will take place under this conditions [1,2]. The rapid solidification processes, RSP, are powerful tools to induce microstructural modifications, which may improve mechanical properties of alloys [2].

The aluminum–Silicon casting alloys (300 series) are being widely used in many automotive components. Alloys of this type combine excellent mechanical properties and high corrosion resistance with good castability. Due the low solid solubility of Fe, Si and Mg in Al, during conventional casting, precipitates of Al_5FeSi, $Al_8Si_6Mg_3Fe$, Mg_2Si and others with more complex structures are formed. However, a substantial increase of solid solubility of those elements in α-Al might be achieved by rapid solidification, which suppresses the formation of those precipitates. The objective of the present study is to analyze the microstructural characteristics and mechanical properties of rapidly solidified A359 aluminum alloy.

2. Experimental procedure

An A359-type alloy with Si 9.4 wt%, Mg 0.7 wt%, Fe 0.12 wt%, Al Bal has been rapidly solidified by melt-spinning using rotating Cu wheel with speed of 56 m/s. The as melt-spun ribbon was produced with 2.7 mm of width and 28–34 μm of thickness. The samples have been characterized by using a combination of optic microscopy, MO, scanning electron microscopy, SEM, and transmission electron microscopy, TEM, with energy dispersive spectroscopy (EDS).

The measurements of both Vickers microhardness and tensile tests were made using an indentaMet-1100–Buehler and Instron-5544, respectively. Both measured were performed at room temperature of as melt-spun ribbons and after heat treatment at 200 and 450 °C ribbons. The tensile tests were performed using at constant crosshead speed of 1.0 mm/min and the length of free ribbon between flat grips was of 40 mm. The grain size was measured using the linear-intercept method, as described in the ASTM E 112-84. The Vickers microhardness tests were measured in the central zone of the cross-section (longitudinal direction) of the ribbon, with the purpose of avoiding border effects, and were performed using a load of 10 gf for 15 s. Each value presented is the result of at least six measurements.

3. Results and discussion

Fig. 1a shows optical cross-section micrograph of the as melt-spun ribbon. The micrograph shows two well defined zones: (i) featureless zone on the wheel side, and (ii) cellular-dendritic central zone with a very fine structure which present a coarsening tendency to the opposite direction to the wheel side. The featureless zone is typical of rapidly quenched alloys and is a result of the extreme grain refinement due to the high cooling rates. TEM analysis of the as melt-spun ribbon central zone (Fig. 1b) shows an equiaxed cellular structure with an average cell size of 0.4–0.7 μm. Hence, using the empirical relation proposed by Matyja et al. [3] of $R = (47/d)^3$ for an Al–11 at%Si alloy, where d is the cell size (in

* Corresponding author. Tel.: +55 16 3351 8545.
E-mail addresses: cartrir@hotmail.com (C. Triveño Rios), peresmm@yahoo.com.br (M.M. Peres), cbolfa@ufscar.br (C. Bolfarini), wjbottaf@ufscar.br (W.J. Botta), kiminami@ufscar.br (C.S. Kiminami).

0925-8388/$ – see front matter © 2010 Published by Elsevier B.V.
doi:10.1016/j.jallcom.2009.12.120

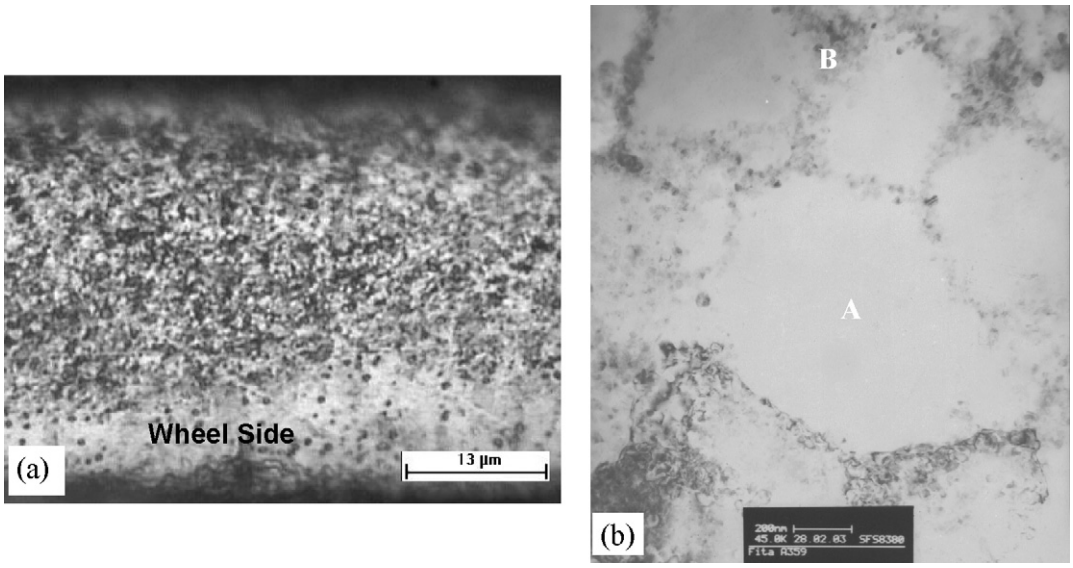

Fig. 1. (a) Optical micrograph of the as melt-spun ribbon cross-section, and (b) Bright field TEM image showing silicon precipitated inside the Al grains and at grain boundaries.

μm) and R the cooling rate, it was possible to calculate the cooling rate (R) between $\sim 3.01 \times 10^5$ and 1.6×10^6 K/s for the A359 alloy processed, that is a typical value for melt-spinning process. The equiaxed cellular structure is composed by silicon particles that preferentially precipitated along the grain boundaries resulting in silicon chains and silicon precipitates distributed inside the α-Al cells without the presence of Mg_2Si metastable phase. The presence of silicon particles along the cell boundaries suggests that some silicon precipitation might have taken place during post-solidification cooling. It is also suggested that the solidification was primarily diffusionless and silicon was entrapped in the Al-matrix. It can be observed the cells centre (region A) without presence of silicon precipitates and cell boundaries with high density of Si precipitates (region B). EDS analysis showed that the silicon content in regions A and B was 2.84 and 14.0–19.0 at%, respectively, and the magnesium content was 0.8 and 1.3 at%, respectively. The average diameter of these Si precipitates is approximately, 19 ± 8 nm. These results are in agreement with the smallest structural refinement obtained in the A359 alloy solidified in cooper mould of varying cross-section involved low cooling rates [4].

In this study it was observed that the silicon grows from nanosize dimensions ($\sim 19 \pm 8$ nm) in the as melt-spun ribbon to

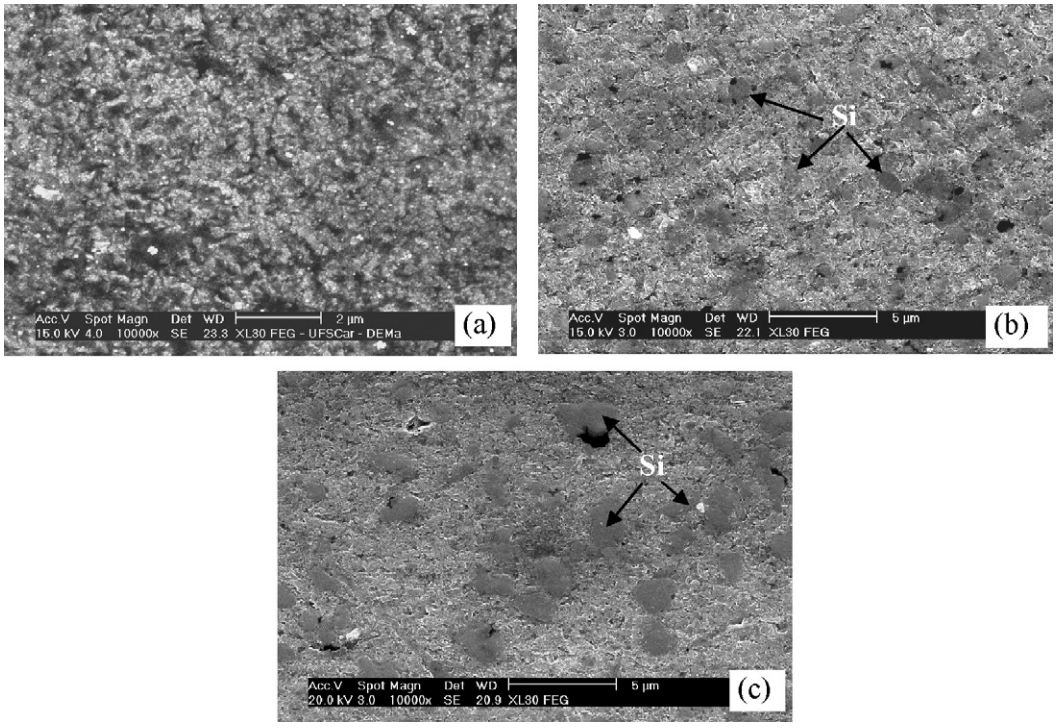

Fig. 2. (a) SEM micrograph after heat treatment for 12 h at: (a) 200 °C, (b) 350 °C, and (c) 450 °C.

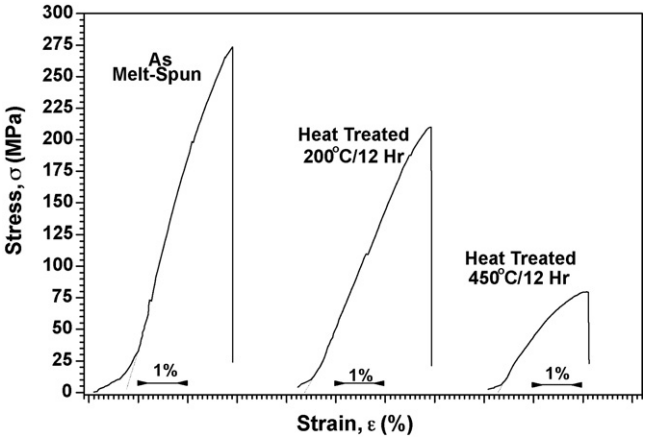

Fig. 3. Stress–strain curves obtained by tensile tests at room temperature for the ribbons.

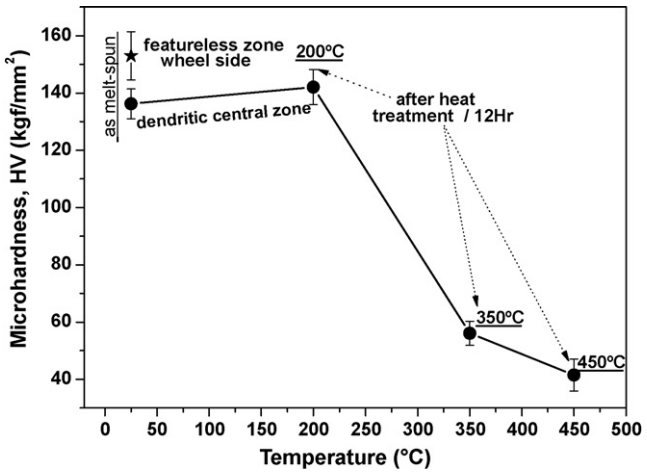

Fig. 4. Measures of Vickers microhardness at room temperature for as melt-spun ribbon and after heat treated at 200, 300 and 450 °C/12 h.

particles with 60–80 nm and $1.7 \pm 0.4\,\mu m$ in diameter in heat treated ribbons by 12 h at 200 and 450 °C, respectively, as observed in Fig. 2. It indicates that at low temperatures of annealing (~200 °C) there was a very low growth rate of the silicon phase. Such behavior changes by increasing the temperature with high growth rates following a power law of time ($t^{1/3}$), through of mainly volume diffusion mechanism [5] or by structural coarsening [6]. Its also suggests a precipitation from a supersaturated Al-matrix occurring between 150 and 190 °C, vanishing the inter-dendrite boundaries [7].

The stress–strain curves are shown in Fig. 3. Apparently the stress–strain relation is almost linear up the fracture in the as melt-spun and annealed at 200 °C samples and less linear in the annealed at 450 °C sample. However, there is only linearity up to a certain elongation beyond which it is curve until fracture without a clear yield point. In general, yield strength (YS) and ultimate tensile strength (UTS) are found to decrease with an increase of heat treatment temperature, due to the microstructural feature changes, such as, intermetallic precipitation, matrix softening, Si particle coarsening, which is related with the strengthen mechanisms. The UTS and YS values differ greatly being 274 and 253, 210 and 202, 79 and 68 MPa for as melt-spun ribbon and after heat treated at 200 and 450 °C, respectively. However, the plastic deformation found in the three samples is small being more characteristic in the annealed at 450 °C sample. The Fig. 4 shows measures of hardness in the cross-section of the ribbons. The hardness of the as melt-spun ribbon was 136.5 kgf/mm^2 and after heat treatment at 200 °C/12 h the hardness increase for 148.1 kgf/mm^2. However, increasing the heat treatment temperature to 450 °C resulted in a reducton of the hardness to 42 kgf/mm^2.

The values of UTS, YS and hardness of the as melt-spun ribbon is superior to the Al–Si alloys produced in permanent mould that presents values of UTS and YS of 98 and 66 MPa for Al–12.6%Si [8], 81 and 58 MPa for Al–7%Si [8], and 234 and 131 MPa for 319.2 alloy with 15 μm of dendrite arm spacing (λ_2) [9], respectively. On the other hand, the hardness of the central cellular-dendritic zone of the as melt-spun ribbon and after heat treatment for 200 °C, it is approximately 2.2 and 2.35 times superior to the conventionally as-cast samples that present a hardness of ~62 kgf/mm^2 for $\lambda_2 = 33\,\mu m$.

The high values of UTS, YS and hardness can be related to the as melt-spun state that consists of a supersaturated solid solution with presence of undissolved solutes in the Al-matrix (Fig. 1b). In this case, the solute atoms affect upon the solvent lattice, as well as, the nature of the operative lattice forces are present owing to the interaction of different atomic species. Another factor, which may contribute is related to internal stresses, which are retained during cooling to room temperature. Such stresses may arise from the difference in thermal expansion of the precipitates and the solvent. The disappearance of this mechanism seems to be responsible by the reduction of UTS and YS in heat treated at 200 °C/12 h ribbon, because internal stresses relaxation process. The increase of hardness in the same sample suggests that the heat treatment at 200 °C for 12 h still corresponds to hardening treatment for A359 alloy. Although these treatments are usually performed at temperatures below 175 °C for Al–Si–Mg alloys [10]. The increase of hardness can be attributed to the precipitation of β″-Mg_2Si particles out of the supersaturated α-Al solid solution, and possibly to the low Mg: Si atomic ratio at rapidly solidified alloys and that probably, it would also increase the real volume fraction of β″-Mg_2Si precipitates [11]. Increasing the heat treatment temperature for 450 °C the hardness it is suddenly reduced for ~42 kgf/mm^2. This value is inferior to the as-cast sample. This reduction is result basically of structural coarsening, reduction of stress level and amount of precipitates.

Fig. 5 shows secondary electron images of the fracture surfaces of the ribbons tested at room temperature. The patterns of fracture in the as melt-spun and after heat treated at 200 °C ribbons can be related as a typical brittle fracture with features of cleavage fracture. The fracture surface of granular cells in the as melt-spun ribbon (Fig. 5a-a1), suggest an intergranular fracture, as resulted of the rapid solidification process. The same fracture type it is observed in the after heat treated at 200 °C ribbon (Fig. 5b-b1), although, be not clear the cracking at grain boundaries due to presence of a more smooth fracture surface. This behavior agrees well with the increase of hardness due to the hardening treatment and precipitation of second phases in the annealed ribbon at 200 °C/12 h. The ribbon after heat treated at 450 °C (Fig. 5c-c1) showed a ductile fracture surface that is characterized by presence of dimples with sizes near to 2 μm superior to the Si particles localized in the inner part of the dimples. It is suggested that the crack propagation takes place through the mechanism of void coalescence (where the voids result from the fracture or removal of the Si particles). The dimple and smooth ripple patterns observed on the fracture surface suggests a transgranular type along the grain boundaries. This result contributes to the decrease of UTS, YS and hardness. Suggesting that an increase of the heat treatment temperature increases the size of the individual precipitate particles while their number decreases resulting in gradual softening of the Al-matrix because to the gradual reduction of the solutes.

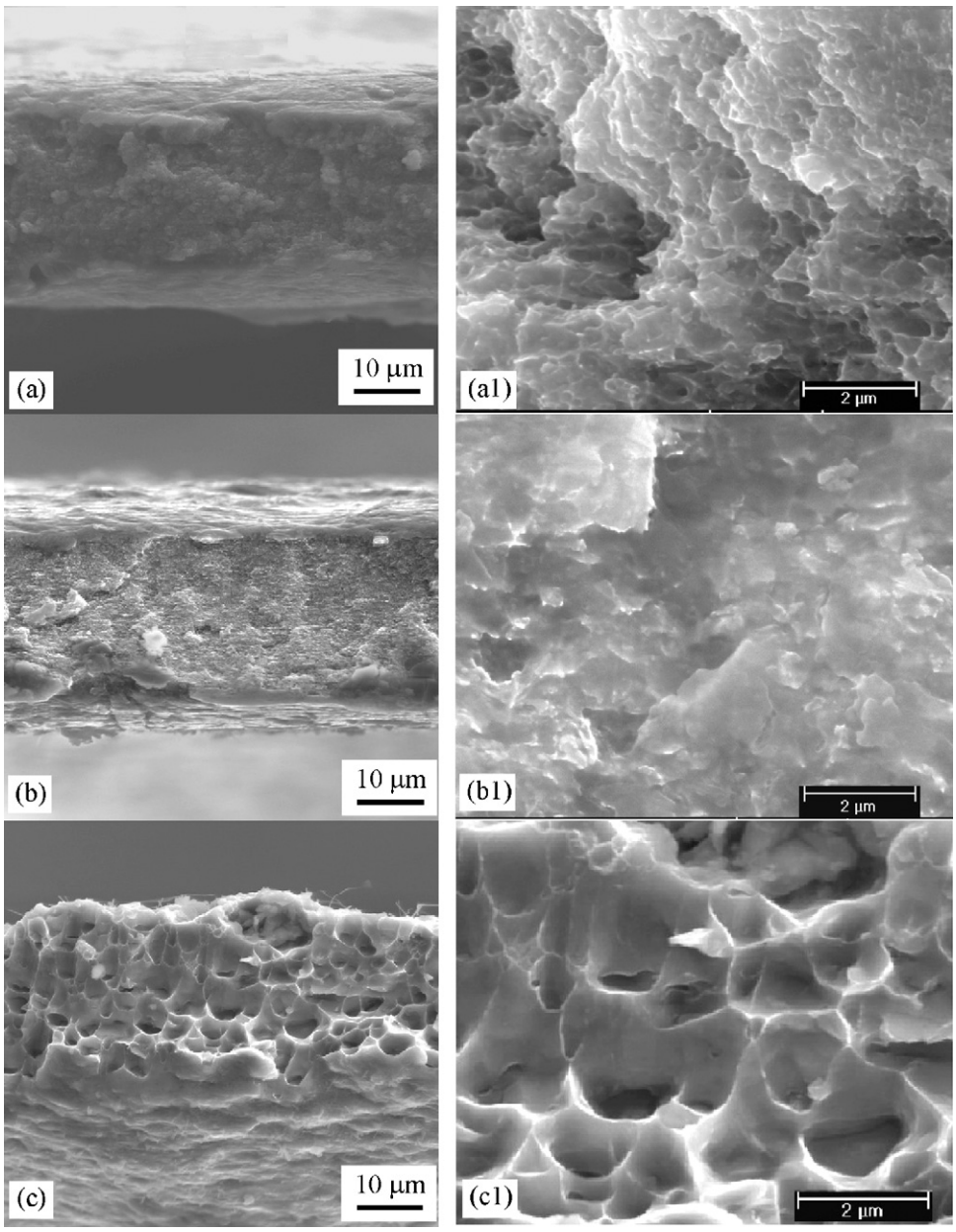

Fig. 5. Fracture surface of tensile test samples prepared from: (a, a1) as melt-spun ribbon, and heat treated ribbons at (b, b1) 200 °C/12 h, and (c, c1) 450 °C/12 h.

4. Conclusions

The microstructural characteristics, hardness and tensile behavior of the A359 ribbon were examined. The transversal sections of the as melt-spun ribbon exhibited a structural refinement with featureless and cellular-grain zones. The grain boundaries are constituted by chains of silicon precipitates and by the grains of supersaturated α-Al solid solution. The cooling rate of the as melt-spun ribbon was estimated between 3.01×10^5 and 1.6×10^6 K/s. Heat treatments of the as melt-spun ribbon promoted the growth of nanosized Si particles from 19 nm to 80 nm (200 °C/12 h) and to 1.72 μm (450 °C/12 h). The improvement in hardness, UTS and YS of the as melt-spun ribbon when compared to the conventionally prepared alloy is related to the amount of silicon in solid solution and to the structural refinement. The decrease of that property after thermal ageing can be attributed to Si precipitation and the subsequent growth of Si particles. But the ductility was not improved as a result of rapid solidification and heat treatments. The as melt-spun and after heat treated at 200 °C ribbons exhibited a cleavage-type brittle fracture different of the after heat treated at 450 °C ribbon, that showed a dimple-type ductile fracture.

Acknowledgements

The authors acknowledge FAPESP and CNPq for the financial support.

References

[1] H. Jones, Mater. Sci. Eng. 65 (1984) 145.
[2] X.Y. Lu, C.D. Cao, B. Wei, Mater. Sci. Eng. A313 (2001) 198.
[3] H. Matyja, B.C. Giessen, N.J. Grant, J. Inst. Met. 96 (1968) 30.

[4] C. Triveño Rios, C. Bolfarini, F.W.J. Botta, C.S. Kiminami, J. Metastable Nanocrystalline Mater. 20–21 (2004) 594.
[5] R.K. Mahanti, K. Lai, A.N. Shiha, C.S. Sivaramakrishnam, Mater. Trans. JIM 34 (1993) 1207.
[6] C. Wagner, Zs. f. Elektrochemie 65 (1961) 581.
[7] N. Stoichev, K. Petrov, S. Yaneva, P. Kovachev, Mater. Sci. Eng. A337 (2002) 12.
[8] L. Qian, H. Toda, S. Nishido, T. Akahori, M. Niinomi, T. Kobayashi, Metall. Mater. Trans. A 36A (2005) 2979.
[9] A.M. Samuel, F.H. Samuel, Metall. Mater. Trans. A 26A (1995) 2359.
[10] D.L. Zhang, Mater. Sci. Forum 217–222 (1996) 771.
[11] J.W. Martin, Micromechanisms in Particle Hardened Alloys, Cambridge University Press, England, 1980, 54.